

Involvement of p53 and p21 in Cellular Defects and Tumorigenesis in *Atm*^{-/-} Mice

YANG XU,^{1*} EVA MARIE YANG,¹ JAMES BRUGAROLAS,² TYLER JACKS,² AND DAVID BALTIMORE³

Department of Biology, University of California, San Diego, La Jolla, California 92093-0322¹; Department of Biology, Massachusetts Institute of Technology, Cambridge, Massachusetts 02139²; and California Institute of Technology, Pasadena, California 91125³

Received 10 March 1998/Accepted 13 April 1998

Disruption of the mouse *Atm* gene, whose human counterpart is consistently mutated in ataxia-telangiectasia (A-T) patients, creates an A-T mouse model exhibiting most of the A-T-related systematic and cellular defects. While ATM plays a major role in signaling the p53 response to DNA strand break damage, *Atm*^{-/-} p53^{-/-} mice develop lymphomas earlier than *Atm*^{-/-} or p53^{-/-} mice, indicating that mutations in these two genes lead to synergy in tumorigenesis. The cell cycle G₁/S checkpoint is abolished in *Atm*^{-/-} p53^{-/-} mouse embryonic fibroblasts (MEFs) following γ -irradiation, suggesting that the partial G₁ cell cycle arrest in *Atm*^{-/-} cells following γ -irradiation is due to the residual p53 response in these cells. In addition, the *Atm*^{-/-} p21^{-/-} MEFs are more severely defective in their cell cycle G₁ arrest following γ -irradiation than *Atm*^{-/-} and p21^{-/-} MEFs. The *Atm*^{-/-} MEFs exhibit multiple cellular proliferative defects in culture, and an increased constitutive level of p21 in these cells might account for these cellular proliferation defects. Consistent with this notion, *Atm*^{-/-} p21^{-/-} MEFs proliferate similarly to wild-type MEFs and exhibit no premature senescence. These cellular proliferative defects are also rescued in *Atm*^{-/-} p53^{-/-} MEFs and little p21 can be detected in these cells, indicating that the abnormal p21 protein level in *Atm*^{-/-} cells is also p53 dependent and leads to the cellular proliferative defects in these cells. However, the p21 mRNA level in *Atm*^{-/-} MEFs is lower than that in *Atm*^{+/+} MEFs, suggesting that the higher level of constitutive p21 protein in *Atm*^{-/-} MEFs is likely due to increased stability of the p21 protein.

Ataxia-telangiectasia (A-T) is an autosomally recessive human genetic disease characterized by pleiotropic defects in multiple systems. Affected patients suffer from growth retardation, neuronal degeneration in the cerebellum leading to ataxia, dilated blood vessels in the eye and facial area, gonadal defects, immunodeficiency, a high incidence of cancer, and hypersensitivity to ionizing radiation (20). Cells derived from A-T patients are defective in their checkpoint responses to ionizing radiation and are hypersensitive to ionizing radiation (22, 27). Following the induction of strand break damage induced by ionizing radiation, normal cells arrest their cell cycle at three cell cycle checkpoints: at the G₁/S border, at S phase, and at the G₂/M border (12). However, all three cell cycle checkpoints in A-T cells are defective in response to ionizing radiation. The cell cycle checkpoint defects of A-T cells have been suggested to account for the cellular hypersensitivity of these cells to ionizing radiation (22, 27).

A gene consistently mutated in A-T patients, denoted *ATM*, has been identified through linkage mapping and positional cloning (9, 26). The *ATM* gene encodes a large kinase which is similar to a family of kinases involved in DNA metabolism and cell cycle checkpoint control in response to DNA damage (26, 34). While the ATM kinase family members contain a kinase domain similar to that of phosphatidylinositol 3-kinase (PI-3 kinase), none of them have been shown to have any lipid kinase activity (13). Instead, a number of ATM family members, including FRAP, DNA-PK, and ATM, display protein kinase activity (3, 4, 11, 16). In addition, immunofluorescence studies using an anti-ATM antibody have shown that ATM is

ubiquitously expressed in all murine tissues and is mainly localized in the nucleus, consistent with the notion that ATM may be involved in the detection of DNA strand break damage and in the activation of cell cycle checkpoints following DNA strand break damage (6).

To clarify the function of ATM and create a mouse model to study the basis of the pleiotropic defects in A-T patients, we disrupted the *Atm* gene in mice through homologous recombinations (33). Mice homozygous for this mutation express most of the A-T phenotypes, including neural degeneration, growth retardation, abolished germ cell development, immune defects, and a high incidence of thymic lymphomas (19, 31). Furthermore, primary cells derived from the *Atm*^{-/-} mice displayed cellular defects characteristic of A-T, including hypersensitivity to γ -irradiation and defective cell cycle G₁/S and S-phase checkpoint control following γ -irradiation (3, 33). In addition, *Atm*^{-/-} mouse embryonic fibroblasts (MEFs) exhibit defective cellular proliferation, inefficient G₁- to S-phase cell cycle progression and premature senescence in culture (33). Similar systematic and cellular defects have been reported in two independently generated *Atm*^{-/-} mouse strains (1, 8). Therefore, *Atm* plays important roles in both cellular responses to strand break damage and normal cellular growth.

p53 is required for the cell cycle G₁ arrest following γ -irradiation (18). The impaired p53 response to γ -irradiation in *Atm*^{-/-} cells could account for the defective cell cycle G₁ arrest in these cells (15, 17, 33). In addition, the increased constitutive level of p21^{CIP1/WAF1} observed in *Atm*^{-/-} MEFs might account for the cellular proliferative defects observed in these mutant cells because p21 is involved in the inhibition of G₁- to S-phase cell cycle progression (5, 7, 30). To test the roles of the defective p53 response and the abnormal p21 protein level in the cellular and developmental defects observed in

* Corresponding author. Mailing address: Department of Biology, University of California, San Diego, Bonner Hall 3430, 9500 Gilman Dr., La Jolla, CA 92093-0322. Phone: (619) 822-1084. Fax: (619) 534-0053. E-mail: yangxu@ucsd.edu.

Atm^{-/-} mice, Atm^{-/-} p21^{-/-} and Atm^{-/-} p53^{-/-} mice were generated.

The majority of Atm^{-/-} p53^{-/-} mice die embryonically. The born double mutant mice are runted and develop lymphomas sometimes of both B and T origin by 2 months of age, indicating a synergy of the Atm and p53 mutations in tumorigenesis since Atm^{-/-} mice develop thymic lymphomas by 4 months of age. Similar to p53^{-/-} cells, Atm^{-/-} p53^{-/-} cells are completely defective in their cell cycle G₁ arrest following γ -irradiation, indicating that the impaired but not abolished p53 response in Atm^{-/-} cells contributes to the partial cell cycle G₁ arrest following γ -irradiation in these cells (33). However, this synergy in tumorigenesis is not observed in Atm^{-/-} p21^{-/-} mice. The development of Atm^{-/-} p21^{-/-} mice is grossly similar to that of Atm^{-/-} mice. However, when compared with wild-type and p21^{-/-} MEFs, the Atm^{-/-} p21^{-/-} MEFs proliferate normally at both low and high passages, consistent with the notion that the increased constitutive level of p21 in Atm^{-/-} MEFs causes the cellular proliferation defects observed in these cells. In addition, because little p21 is observed in Atm^{-/-} p53^{-/-} MEFs, the increased p21 protein level in Atm^{-/-} MEFs is p53 dependent and likely due to a more stable p21 protein, because the p21 mRNA level in Atm^{-/-} MEFs is lower instead of higher than that in Atm^{+/+} MEFs.

MATERIALS AND METHODS

Generation of Atm^{-/-} p21^{-/-} and Atm^{-/-} p53^{-/-} mice. The p21^{-/-} and p53^{-/-} mice were described previously (5, 14). Because Atm^{-/-} mice are sterile (31), the p21^{-/-} mice were bred with Atm^{+/+} mice to generate Atm^{+/+} p21^{-/-} mice, which were intercrossed to generate Atm^{-/-} p21^{-/-} mice. The Atm^{+/+} p21^{-/-} mice were then intercrossed to generate Atm^{-/-} p21^{-/-} mice. A similar breeding scheme was attempted to generate Atm^{-/-} p53^{-/-} mice but attempts to intercross Atm^{+/+} p53^{-/-} mice have failed. So Atm^{+/+} p53^{-/-} mice were intercrossed instead to generate Atm^{-/-} p53^{-/-} mice.

Flow cytometric analysis of thymocytes. Thymi were surgically removed from mice and single-cell suspensions were prepared as previously described (31). For two-color flow cytometric analysis, one-half million cells were simultaneously stained with phycoerythrin-conjugated anti-CD4 antibody and fluorescein isothiocyanate (FITC)-conjugated anti-CD8 antibody. After being washed with staining buffer (3% fetal bovine serum [FBS] in phosphate-buffered saline [PBS]), stained cells were analyzed using a FACScan (Becton-Dickinson) and CellQuest software. All antibodies were obtained from Pharmingen.

Generation and culture of MEFs. MEFs were derived from day 14 or day 16 embryos as previously described (33). The Atm^{-/-} p21^{-/-} or Atm^{-/-} p53^{-/-} MEFs were derived from embryos obtained through the intercrosses of Atm^{+/+} p21^{-/-} mice or Atm^{+/+} p53^{-/-} mice, respectively. MEFs were cultured in Dulbecco's modified Eagle's medium (DMEM) supplemented with 10% fetal calf serum, 5 mM glutamine, 50 μ M β -mecaptoethanol, 50 U of penicillin per ml, and 50 U of streptomycin per ml at 37°C with 5% CO₂.

γ -Irradiation treatment of MEFs and cell cycle analysis. MEFs were synchronized at the G₀ phase of the cell cycle by culturing in medium supplemented with 0.1% FBS for 96 h as previously described (7). The G₀-synchronized cells were trypsinized and irradiated in suspension with a ¹³⁷Cs γ -ray source. Subsequently, the irradiated and untreated MEFs were plated in 10-cm-diameter plates at a density of 0.8 \times 10⁶ to 1 \times 10⁶ cells/plate in normal growth medium supplemented with 10 μ M bromodeoxyuridine (BrdU). After 24 h of BrdU labeling, cells were harvested, fixed in 70% ethanol, and stored at -20°C until analysis.

The analyses of DNA content and synthesis were performed as previously described (33). DNA content was revealed by staining with propidium iodide, and DNA synthesis was revealed by staining with FITC-conjugated anti-BrdU antibody (Southern Biotech., Inc.). The stained cells were analyzed using a FACScan and the CellQuest program as previously described (33).

Northern blot analysis. Total RNA was prepared from harvested MEFs with Trizol reagent (Sigma) according to the manufacturer's protocol. Total RNA (15 μ g) was electrophoresed on a 17.5% formaldehyde-1% agarose gel and was transferred to a nylon membrane (Amersham) as previously described (32). The full-length mouse p21 cDNA was used as a probe to hybridize to the membrane as previously described (21). To standardize the amount of RNA loaded into each lane, the same filter was stripped and hybridized with a glyceraldehyde-3-phosphate dehydrogenase (GAPDH) probe as previously described (32). The hybridized filter was sequentially exposed to both X-ray films and PhosphorImager screens. The amount of p21 and GAPDH mRNA in each sample was quantitated with an ImageQuant program (Molecular Dynamics).

Assays for in vitro cellular proliferation and G₁/S cell cycle progression. Cellular proliferation assays were performed as previously described (7, 33).

Briefly, 10⁵ MEFs were plated onto each 35-mm-diameter plate, and each day after plating, MEFs from three plates of each genotype were trypsinized and counted with a hemacytometer. To synchronize MEFs at G₀, a subconfluent culture was washed with PBS and placed in DMEM containing 0.1% FBS for 96 h (7). The synchronized MEFs were harvested and released into DMEM supplemented with 10% FBS and 10 μ M BrdU for 24 h. Cells in S phase were analyzed using flow cytometry as described above.

Western blot analysis. Western blot analysis of p21 protein levels in MEFs was performed as previously described (33). Protein extracts derived from 3 \times 10⁵ cells were loaded into each lane, separated by sodium dodecyl sulfate-12% polyacrylamide gel electrophoresis, and transferred to nitrocellulose membranes (Schleicher and Schuell). The filter was probed with a polyclonal rabbit anti-p21 antibody obtained from Santa Cruz Biochemicals, and then was incubated with horseradish peroxidase-conjugated secondary antibody and developed with enhanced chemiluminescence (Amersham). To verify that an equivalent amount of protein was loaded into each lane, the same filter was subsequently probed with a polyclonal rabbit anti-tubulin antibody (ICN Biomedicals, Inc.) and developed as described above.

RESULTS

Developmental phenotypes in Atm^{-/-} p53^{-/-} and Atm^{-/-} p21^{-/-} mice. Because p53^{-/-} Atm^{+/+} mice are not healthy and usually develop testicular sarcomas, attempts to use these mice to generate Atm^{-/-} p53^{-/-} mice have failed so far. (Testicular sarcomas are also a common malignancy found in the strain of p53^{-/-} mice that we used [14].) Therefore, Atm^{+/+} p53^{-/-} mice were intercrossed to generate Atm^{-/-} p53^{-/-} mice. While the predicted frequency of Atm^{-/-} p53^{-/-} mice in the offspring of this intercross should be 1/16, only about 2% of over 350 offspring genotyped were Atm^{-/-} p53^{-/-} mice, suggesting that about 60% of these double mutant mice die prenatally. In addition, the born Atm^{-/-} p53^{-/-} mice are apparently runted at the weaning age and thus the prevalence of growth retardation phenotypes is hard to judge.

To generate Atm^{-/-} p21^{-/-} mice, Atm^{+/+} p21^{-/-} mice were generated and intercrossed. Consistent with the predicted frequency of 1/4, about 25% of the offspring from the Atm^{+/+} p21^{-/-} crosses were double mutant animals, indicating that there is no prenatal death during the early development of the double mutant mice (data not shown).

Atm^{-/-} mice exhibit several developmental defects, including growth retardation and defective T-cell development (31). While the Atm^{-/-} p53^{-/-} mice are runted and appear unhealthy by the weaning age, the Atm^{-/-} p21^{-/-} mice are healthy at this stage of development and were studied for this spectrum of developmental defects. Similar to Atm^{-/-} mice (31), the 1- to 2-month-old Atm^{-/-} p21^{-/-} mice are also growth retarded with a body weight about 79% \pm 7% of that of the p21^{-/-} control mice (data derived from six sets of Atm^{-/-} p21^{-/-} and Atm^{+/+} p21^{-/-} mice).

T-cell developments in Atm^{-/-} p21^{-/-} mice were analyzed using flow cytometry and cell counting. While the total number of thymocytes in Atm^{-/-} mice is on average 40% \pm 10% of that of Atm^{+/+} control mice (33), the total number of thymocytes in the Atm^{-/-} p53^{-/-} and Atm^{-/-} p21^{-/-} mice in this study averaged 50% \pm 5% and 52% \pm 12%, respectively, of those of p53^{-/-} and p21^{-/-} control mice (data derived from four sets of Atm^{-/-} p53^{-/-} and p53^{-/-} control mice and seven sets of 1- to 2-month-old Atm^{-/-} p21^{-/-} and Atm^{+/+} p21^{-/-} control mice). In addition, when determined by flow cytometry for the expression of CD4 and CD8 surface markers, CD4⁺ and CD8⁺ single-positive mature thymocytes were still significantly reduced in the thymi of Atm^{-/-} p21^{-/-} and Atm^{-/-} p53^{-/-} mice compared to those of Atm^{+/+} p21^{-/-} and Atm^{+/+} p53^{-/-} control mice, respectively (Fig. 1). Therefore, the thymocyte differentiation from the CD4⁺ CD8⁺ stage to the CD4⁺ or CD8⁺ stage is consistently defective in Atm^{-/-}, Atm^{-/-} p21^{-/-}, and Atm^{-/-} p53^{-/-} mice.

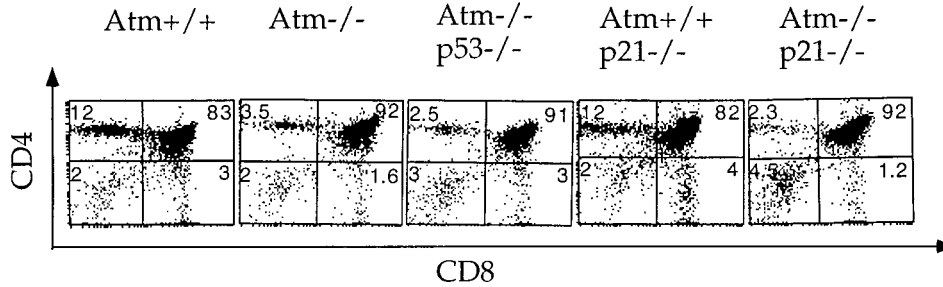


FIG. 1. Flow cytometric analysis of T-cell development in 1- to 2-month-old *Atm*^{+/+}, *Atm*^{-/-}, *Atm*^{-/-} *p53*^{-/-}, *Atm*^{+/+} *p21*^{-/-}, and *Atm*^{-/-} *p21*^{-/-} mice. Cells residing in the lymphoid gate were analyzed and the percentages of total cells in a particular gate are indicated. Consistent data were obtained from two *Atm*^{-/-} *p53*^{-/-} mice and seven sets of *Atm*^{+/+} *p21*^{-/-} and *Atm*^{-/-} *p21*^{-/-} mice.

Lymphomas in *Atm*^{-/-} *p53*^{-/-} and *Atm*^{-/-} *p21*^{-/-} mice.

While *Atm*^{-/-} mice invariably develop thymic lymphomas by 4 months of age, seven *Atm*^{-/-} *p53*^{-/-} mice developed thymic and/or peripheral lymphomas by 2 months of age. When analyzed with flow cytometry, three of the seven lymphomas derived from *Atm*^{-/-} *p53*^{-/-} mice appear to have been composed of two populations of tumor cells of different sizes (Fig. 2A). When the analysis was gated on these two populations of tumor cells, the smaller tumor cells appeared to be mainly composed of B220⁺ cells, which are also Thy-1⁻ CD4⁻, indicating that they are phenotypically of B-cell origin (Fig. 2B and data not shown). The larger tumor cells expressed some T-cell markers, including CD4 and Thy-1, but were B220⁻, suggesting that they were of T-cell origin (Fig. 2B and data not shown). Therefore, the *Atm*^{-/-} *p53*^{-/-} mice can develop lymphomas of both B- and T-cell origin.

Similar to *Atm*^{-/-} mice, *Atm*^{-/-} *p21*^{-/-} mice invariably develop thymic lymphomas by 5 months of age, and no other

malignancies have been detected in these animals at an elevated frequency. In addition, similar to the thymic lymphoma cells derived from *Atm*^{-/-} mice, the thymic lymphoma cells observed in *Atm*^{-/-} *p21*^{-/-} mice are mostly of CD4⁺ CD8⁺ immature T-cell origin (data not shown) (31).

Cell cycle G₁ arrest following γ -irradiation in *Atm*^{-/-} *p53*^{-/-} and *Atm*^{-/-} *p21*^{-/-} MEFs. In response to γ -irradiation, *Atm*^{-/-} MEFs are partially defective in their cell cycle G₁ arrest, presumably due to a greatly reduced and delayed p53 upregulation in response to γ -irradiation (33). In addition, the constitutively higher basal protein level of p21 in *Atm*^{-/-} MEFs might also affect the cell cycle G₁ arrest of these cells in response to γ -irradiation (33). To test these possibilities, the cell cycle G₁ arrest following γ -irradiation in *Atm*^{-/-} *p53*^{-/-} and *Atm*^{-/-} *p21*^{-/-} MEFs was evaluated as previously described (7). Briefly, MEFs synchronized at G₀ by serum starvation were treated with 0 or 10 Gy of γ irradiation and released into medium supplemented with 10% FBS and 10 μ M BrdU. After 24 h, the percentages of S-phase cells in the irradiated and untreated MEFs were assayed with flow cytometry as previously described (31) (Fig. 3A). Following γ -irradiation, there is essentially no cell cycle G₁ arrest in *p53*^{-/-} and *p53*^{-/-} *Atm*^{-/-} MEFs while there is more than 50% reduction of S-phase cells in wild-type MEFs (Fig. 3B). In addition, the *Atm*^{-/-} *p21*^{-/-} MEFs are more severely defective in their cell cycle G₁ arrest following γ -irradiation than *p21*^{-/-} and *Atm*^{-/-} MEFs (Fig. 3B).

Growth properties of *Atm*^{-/-} *p21*^{-/-} and *Atm*^{-/-} *p53*^{-/-} MEFs. The *Atm*^{-/-} MEFs exhibit defects in cellular proliferation, including slower proliferation rate, lower saturation density, inefficient G₁- to S-phase cell cycle progression, and premature senescence, possibly due to the increased basal level of p21 in these mutant cells (33). Therefore, the cellular proliferation of *Atm*^{-/-} *p21*^{-/-} and *Atm*^{-/-} *p53*^{-/-} MEFs were examined as previously described (33). At earlier passages, *Atm*^{-/-} *p21*^{-/-}, *Atm*^{-/-} *p53*^{-/-}, *p21*^{-/-}, and wild-type MEFs proliferate similarly and reach similar saturation densities, while as expected, *Atm*^{-/-} MEFs proliferate more slowly (Fig. 4A). In addition, *Atm*^{-/-} *p21*^{-/-} and *Atm*^{-/-} *p53*^{-/-} MEFs are capable of proliferating at high passages (passage 6), while *Atm*^{-/-} MEFs are senescent (data not shown) (26, 33).

The cell cycle G₁- to S-phase progression was examined as previously described (33). *Atm*^{+/+}, *Atm*^{+/+} *p21*^{-/-}, *Atm*^{-/-} *p21*^{-/-}, *Atm*^{+/+} *p53*^{-/-}, and *Atm*^{-/-} *p53*^{-/-} MEFs synchronized at G₀ through serum starvation were serum stimulated for 24 h, and the percentages of cells in S phase were determined with flow cytometry. Similar percentages of S-phase cells were detected in all the MEF samples tested (Fig. 4B). Therefore, all the cellular proliferation defects tested in

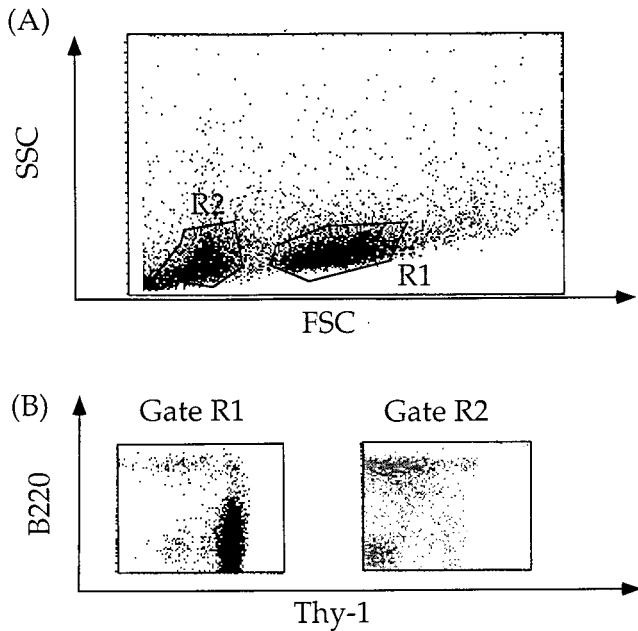


FIG. 2. FACScan profile of lymphomas in *Atm*^{-/-} *p53*^{-/-} mice. Peripheral lymphomas derived from a 6-week-old *Atm*^{-/-} *p53*^{-/-} mouse were analyzed for cell size (A) and surface expression of pan-T-cell marker Thy-1 and pan-B-cell marker B220 (B). The plot of the forward scatter (FSC) versus the sizing scatter (SSC) indicates two populations of uniform lymphoma cells in the tumor, as indicated by R1 and R2 gates.

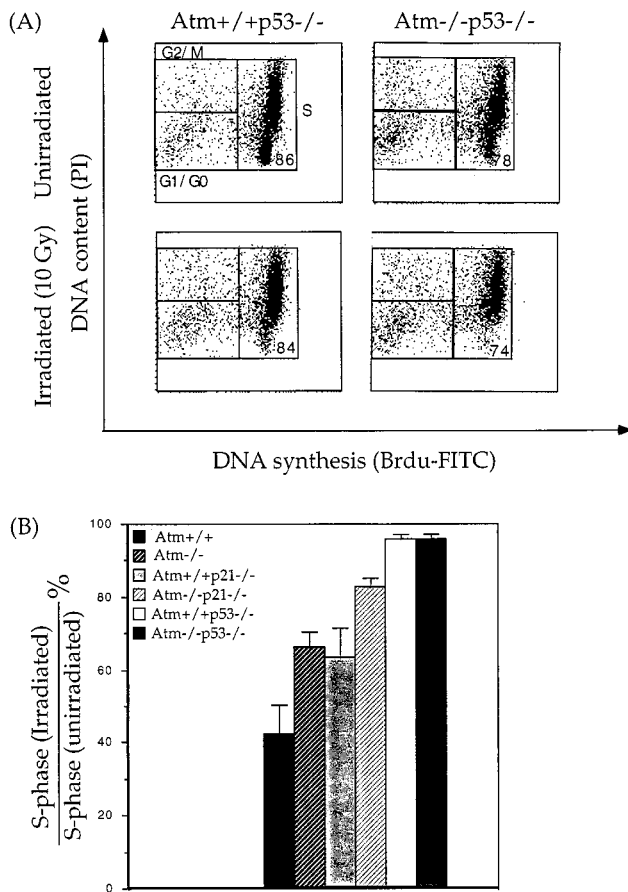


FIG. 3. Cell cycle G₁ arrest following γ -irradiation in MEFs of various genotypes. (A) Representative FACScan profile of untreated and irradiated *Atm*^{+/+} *p53*^{-/-} and *Atm*^{-/-} *p53*^{-/-} MEFs. The 2N and 4N DNA contents were revealed by propidium iodide (PI) staining, and DNA synthesis was revealed by staining with FITC-conjugated anti-BrdU antibody. Cells residing in G₀/G₁, S, and G₂/M phases are indicated by boxes. The percentages of S-phase cells are also indicated. (B) Quantitative analysis of the reduction of S-phase cells following γ -irradiation in *Atm*^{+/+}, *Atm*^{+/+} *p21*^{-/-}, *Atm*^{-/-} *p21*^{-/-}, *Atm*^{+/+} *p53*^{-/-}, and *Atm*^{-/-} *p53*^{-/-} MEFs. Two independent experiments were performed and in each experiment, three irradiated samples of MEFs of each genotype (except in the case of *Atm*^{-/-} MEFs, for which one set of samples is involved) and untreated controls were compared. Mean values with standard deviations (indicated by error bars) are presented.

Atm^{-/-} MEFs are rescued in *Atm*^{-/-} *p53*^{-/-} and *Atm*^{-/-} *p21*^{-/-} MEFs.

p21 protein and mRNA levels in various MEFs. To test whether the increased basal protein level of p21 in *Atm*^{-/-} mice is dependent on p53, the p21 protein level in *Atm*^{-/-} *p53*^{-/-} MEFs was analyzed by Western blotting. As described previously, a much higher level of p21 was detected in *Atm*^{-/-} MEFs than *Atm*^{+/+} MEFs (Fig. 5A) (31). However, little p21 protein was detected in both *p53*^{-/-} and *Atm*^{-/-} *p53*^{-/-} MEFs (Fig. 5A). As expected, no p21 could be detected in *Atm*^{-/-} *p21*^{-/-} and *Atm*^{+/+} *p21*^{-/-} MEFs (Fig. 5A).

To test whether the increased level of p21 protein in *Atm*^{-/-} MEFs is due to a higher level of p21 mRNA in these cells, total RNA was prepared from passage 3 *Atm*^{-/-} and *Atm*^{+/+} control MEFs and analyzed by Northern blotting using the full-length mouse p21 cDNA as a probe (21). While the p21 mRNA could be easily identified in both *Atm*^{+/+} and *Atm*^{-/-} MEF samples, a lower p21 mRNA level was detected in the *Atm*^{-/-} MEF samples compared to that of *Atm*^{+/+} MEF controls derived from the same pregnant female, indicating

that the increased level of constitutive p21 protein in *Atm*^{-/-} MEFs is not due to the higher p21 mRNA level in these cells (Fig. 5B). Consistent data were obtained from an additional two sets of *Atm*^{+/+} and *Atm*^{-/-} MEFs (data not shown).

DISCUSSION

Atm^{-/-} cells show an impaired p53 upregulation in response to γ -irradiation and an increased level of p21, either or both of which could be responsible for their cellular defects and increased tumorigenesis. To study this issue, we generated *Atm*^{-/-} *p53*^{-/-} and *Atm*^{-/-} *p21*^{-/-} mice and derived MEFs from them. The cellular proliferative defects observed in *Atm*^{-/-} MEFs are absent in *Atm*^{-/-} *p21*^{-/-} and *Atm*^{-/-} *p53*^{-/-} MEFs. In addition, the cell cycle G₁ checkpoint response to γ -irradiation is more severely defective in *Atm*^{-/-} *p53*^{-/-} and *Atm*^{-/-} *p21*^{-/-} MEFs than in *Atm*^{-/-} MEFs. While the developmental defects and tumorigenesis in the *Atm*^{-/-} *p21*^{-/-} mice are similar to those in *Atm*^{-/-} mice, the majority of *Atm*^{-/-} *p53*^{-/-} mice die prenatally and the surviving *Atm*^{-/-} *p53*^{-/-} mice develop tumors earlier than the *Atm*^{-/-} and *p53*^{-/-} mice, suggesting a cooperation of *Atm* and *p53* in mouse embryonic development as well as in tumor suppression.

An increased p21 protein level can inhibit cell cycle G₁/S transition and is also correlated with cellular senescence (10, 23–25, 30). Therefore, an increased constitutive p21 protein level in *Atm*^{-/-} MEFs could account for the cellular proliferative defects, including slower proliferation, inefficient cell cycle G₁/S progression, and premature senescence (33). Consistent with this notion, none of the cellular proliferative defects observed in *Atm*^{-/-} MEFs were evident in *Atm*^{-/-} *p21*^{-/-} MEFs, indicating that the increased constitutive p21 level is indeed responsible for the cellular proliferative defects observed in *Atm*^{-/-} cells. In addition, the proliferative defects observed in *Atm*^{-/-} MEFs are also rescued in *Atm*^{-/-} *p53*^{-/-} MEFs, probably due to the fact that a minimum level of p21 is expressed in any *p53*^{-/-} MEFs. Thus, the p21 expression in cycling *Atm*^{-/-} MEFs is apparently p53 dependent, just as it is in wild-type cells. Since in normal-cycling MEFs, p53 is thought to transcriptionally activate p21 mRNA expression through binding to the two p53 binding sites in the p21 promoter region, the regulation of p21 expression by p53 in *Atm*^{-/-} MEFs is most likely at the transcriptional level (21).

The increased p21 level in the *Atm*^{-/-} MEFs might be due to either a higher basal activity of the p53-p21 pathway leading to an increased level of p21 mRNA or a more stable p21 protein in the *Atm*^{-/-} MEFs. However, a lower level of p21 mRNA was detected in the *Atm*^{-/-} MEFs than in the *Atm*^{+/+} control MEFs, indicating that the higher level of constitutive p21 protein in the *Atm*^{-/-} MEFs is not due to a higher p21 mRNA level in these cells but is likely due to the increased stability of p21 protein in these cells. This finding is also consistent with the notion that ATM might be involved in the maintenance of the p53 protein level not only after excessive DNA damage but also during normal cellular proliferation.

While the cellular proliferative defects in *Atm*^{-/-} cells are rescued in *Atm*^{-/-} *p21*^{-/-} cells, the growth retardation observed in *Atm*^{-/-} mice is not rescued in the *Atm*^{-/-} *p21*^{-/-} mice because these double mutant mice are still smaller than their *p21*^{-/-} control littermates. Therefore, the growth retardation in *Atm*^{-/-} mice cannot be due solely to the cellular proliferative defects in *Atm*^{-/-} cells. Instead, other potential defects, such as the abnormal production of growth factors due to the neural defects in *Atm*^{-/-} mice, might account for the growth retardation in *Atm*^{-/-} mice (19). In addition, there is

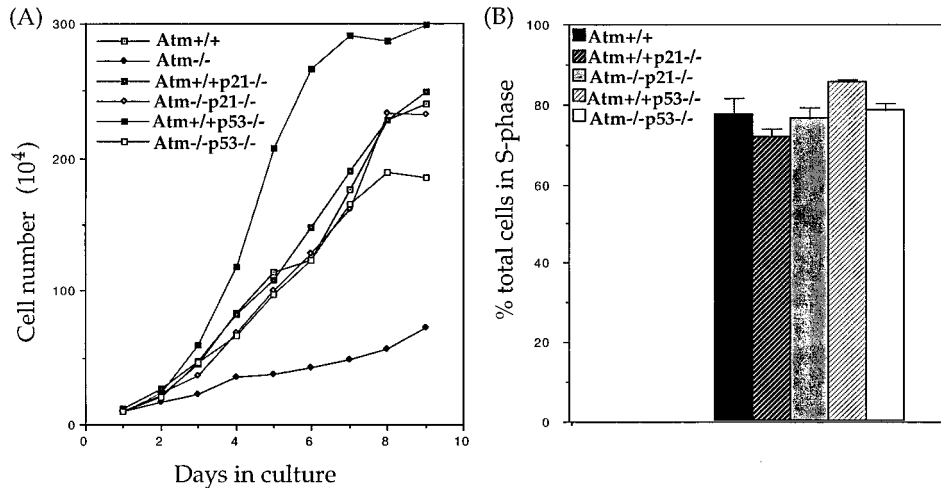


FIG. 4. In vitro cellular proliferation and G₁/S-phase cell cycle progression following serum stimulation of MEFs of various genotypes. (A) Proliferation curves and saturation densities of *Atm*^{+/+}, *Atm*^{-/-}, *Atm*^{+/+} *p21*^{-/-}, *Atm*^{-/-} *p21*^{-/-}, *Atm*^{+/+} *p53*^{-/-}, and *Atm*^{-/-} *p53*^{-/-} MEFs at passage 3. The cell numbers represent the averages of three plates counted at each time point. (B) Quantitative analysis of the percentage of S-phase cells after serum stimulation for 24 h of G₀-synchronized *Atm*^{+/+}, *Atm*^{+/+} *p21*^{-/-}, *Atm*^{-/-} *p21*^{-/-}, *Atm*^{+/+} *p53*^{-/-}, and *Atm*^{-/-} *p53*^{-/-} MEFs. The BrdU-labeled MEFs were analyzed with flow cytometry, and the S-phase cells were revealed by staining with anti-BrdU antibody. Three independent experiments were performed and the mean values with standard derivations (indicated by error bars) are presented.

a significant reduction of the total number of thymocytes in *Atm*^{-/-} mice, possibly due to defective thymocyte proliferation or impaired V(D)J recombination or both (31). However, in contrast to the findings obtained for the *Atm*^{-/-} *p21*^{-/-} and

Atm^{-/-} *p53*^{-/-} MEFs, there is no apparent rescue of thymus cellularity in the *Atm*^{-/-} *p21*^{-/-} and *Atm*^{-/-} *p53*^{-/-} mice, indicating that p53 and p21 are not involved in the thymus hypoplasia in *Atm*^{-/-} mice. However, this does not rule out the possibility that defective thymocyte proliferation contributes to the thymus hypoplasia in *Atm*^{-/-} mice.

The cell cycle G₁ arrest following γ -irradiation is abolished in *p53*^{-/-} MEFs but is partially defective in *Atm*^{-/-} MEFs (15, 17, 18, 33). Consistent with the notion that the cell cycle G₁ arrest in response to γ -irradiation is p53 dependent (18), the p53 upregulation in response to γ -irradiation in *Atm*^{-/-} cells is greatly impaired and delayed (15, 17, 33). Therefore, our findings that *Atm*^{-/-} *p53*^{-/-} MEFs are completely deficient in their cell cycle G₁ arrest in response to γ -irradiation indicate that the residual p53 response to γ -irradiation in *Atm*^{-/-} cells contributes to the partial G₁ cell cycle arrest in *Atm*^{-/-} MEFs. Thus, in response to DNA strand break damage, ATM plays a major role in signaling the p53 upregulation but there exist ATM-independent signaling pathways that can partially compensate for this ATM activity.

While ATM plays a major role in signaling the p53 response to γ -irradiation, the *Atm*^{-/-} *p53*^{-/-} mice develop lymphomas earlier than *Atm*^{-/-} mice, indicating that mutations in these two genes can cooperate in tumorigenesis. Two observations could account for this synergy in tumorigenesis. First, the cell cycle checkpoint defects occurring in response to DNA damage induced by γ -irradiation are more severe in *Atm*^{-/-} *p53*^{-/-} cells than in *Atm*^{-/-} cells. Secondly, the p53-dependent apoptosis of thymocytes in response to γ -irradiation is only partially defective in *Atm*^{-/-} thymocytes but is completely abolished in *Atm*^{-/-} *p53*^{-/-} cells (29, 33). In addition, ATM signals the upregulation of p53 only in response to DNA strand break damage but is not involved in such signaling in the cellular responses to DNA damage induced by UV or base mismatch (33, 33a). Therefore, while only the cellular response to DNA strand break damage is defective in *Atm*^{-/-} cells, cellular responses to multiple forms of DNA damage and other cellular stresses are defective in *Atm*^{-/-} *p53*^{-/-} cells, thus providing the potential basis for the synergy of tumorigenesis

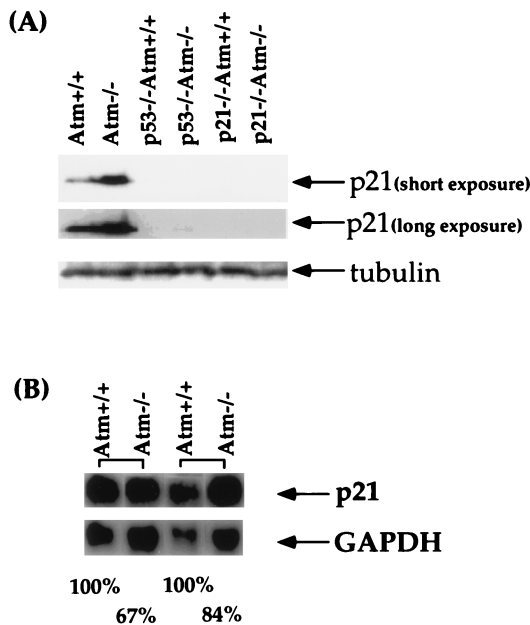


FIG. 5. p21 protein and mRNA levels in MEFs of various genotypes. (A) p21 protein levels in *Atm*^{+/+}, *Atm*^{-/-}, *Atm*^{+/+} *p53*^{-/-}, *Atm*^{-/-} *p53*^{-/-}, *Atm*^{+/+} *p21*^{-/-}, and *Atm*^{-/-} *p21*^{-/-} MEFs. Both the short exposure and the long exposure of the same Western blot are presented. The genotypes are shown at the top. p21 and the β -tubulin are indicated by arrows. (B) p21 mRNA levels in *Atm*^{-/-} and *Atm*^{+/+} control MEFs. The p21 mRNA and loading control GAPDH are indicated by arrows. The genotypes are indicated at the top. The levels of p21 and GAPDH mRNA in each sample were quantitated using an ImageQuant program with a PhosphorImager (Molecular Dynamics). After the p21 mRNA level of each sample was standardized with its GAPDH mRNA level, the percentile ratio of the p21 mRNA level in *Atm*^{-/-} MEFs versus that in *Atm*^{+/+} MEF controls was determined and is indicated at the bottom.

in $Atm^{-/-}$ $p53^{-/-}$ mice. The $Atm^{-/-}$ $p53^{-/-}$ mice also develop lymphomas earlier than $p53^{-/-}$ mice (14). Therefore, other defective but $p53$ -independent cellular responses to strand break damage in $Atm^{-/-}$ cells, such as the defective S-phase cell cycle checkpoint which occurs in response to strand break damage, can account for the earlier onset of tumors in $Atm^{-/-}$ $p53^{-/-}$ mice (3).

An independently generated $Atm^{-/-}$ $p53^{-/-}$ mouse line was reported while this paper was in preparation (29). The findings for our $Atm^{-/-}$ $p53^{-/-}$ mice are in general agreement with those for the reported mouse line. While this paper was being reviewed, two reports described the meiosis, tumorigenesis, and apoptosis responses in two independently generated $Atm^{-/-}$ $p21^{-/-}$ mouse lines (2, 28).

ACKNOWLEDGMENTS

This project was partially supported by a National Institute of Health grant to D.B. and grants from AT Childrens Projects to D.B. and Y.X. Y.X. was partly supported by the Cancer Research Fund of the Damon Runyon-Walter Winchell Foundation. D.B. is an American Cancer Society Research Professor.

REFERENCES

- Barlow, C., S. Hirotsune, R. Paylor, M. Liyanage, M. Eckhaus, F. Collins, Y. Shiloh, J. N. Crawley, T. Ried, D. Tagle, and A. Wynshaw-Boris. 1996. *Atm*-deficient mice: a paradigm of ataxia telangiectasia. *Cell* **86**:159–171.
- Barlow, C., M. Liyanage, P. B. Moens, C. X. Deng, T. Ried, and A. Wynshaw-Boris. 1997. Partial rescue of the prophase I defects of *Atm*-deficient mice by $p53$ and $p21$ null alleles. *Nat. Genet.* **17**:462–466.
- Baskaran, R., L. D. Wood, L. L. Whitaker, C. E. Connon, S. E. Morgan, Y. Xu, C. Barlow, D. Baltimore, A. Wynshaw-Boris, M. B. Kastan, and J. Y. Wang. 1997. Ataxia telangiectasia mutant protein activates c-Abl tyrosine kinase in response to ionizing radiation. *Nature* **387**:516–519.
- Brown, E. J., P. A. Beal, C. T. Keith, J. Chen, T. B. Shin, and S. L. Schreiber. 1995. Control of $p70$ $s6$ kinase by kinase activity of FRAP in vivo. *Nature* **377**:441–446.
- Brugarolas, J., C. Chandrasekaran, J. I. Gordon, D. Beach, T. Jacks, and G. J. Hannon. 1995. Radiation-induced cell cycle arrest compromised by $p21$ deficiency. *Nature* **377**:552–557.
- Chen, G., and E. Lee. 1996. The product of the *ATM* gene is a 370-kDa nuclear phosphoprotein. *J. Biol. Chem.* **271**:33693–33697.
- Deng, C., P. Zhang, J. W. Harper, S. J. Elledge, and P. Leder. 1995. Mice lacking $p21^{Cip1}/WAF1$ undergo normal development, but are defective in G1 checkpoint control. *Cell* **82**:675–684.
- Elson, A., Y. Wang, C. J. Daugherty, C. C. Morton, F. Zhou, J. Campos-Torres, and P. Leder. 1996. Pleiotropic defects in ataxia-telangiectasia protein-deficient mice. *Proc. Natl. Acad. Sci. USA* **93**:13084–13089.
- Gatti, R. A., et al. 1988. Localization of an ataxia-telangiectasia gene to chromosome 11q22–23. *Nature* **336**:577–580.
- Halevy, O., B. G. Novitch, D. B. Spicer, S. X. Skapek, J. Rhee, G. J. Hannon, D. Beach, and A. B. Lassar. 1995. Correlation of terminal cell cycle arrest of skeletal muscle with induction of $p21$ by MyoD. *Science* **267**:1018–1021.
- Hartley, K. O., D. Gell, G. C. Smith, H. Zhang, N. Divecha, M. A. Connelly, A. Admon, S. P. Lees-Miller, C. W. Anderson, and S. P. Jackson. 1995. DNA-dependent protein kinase catalytic subunit: a relative of phosphatidylinositol 3-kinase and the ataxia telangiectasia gene product. *Cell* **82**:849–856.
- Hartwell, L. H., and M. B. Kastan. 1994. Cell cycle control and cancer. *Science* **266**:1821–1828.
- Hunter, T. 1995. When is a lipid kinase not a lipid kinase? When it is a protein kinase. *Cell* **83**:1–4.
- Jacks, T., L. Remington, B. O. Williams, E. M. Schmitt, S. Halachmi, R. T. Bronson, and R. A. Weinberg. 1994. Tumor spectrum analysis in $p53$ -mutant mice. *Curr. Biol.* **4**:1–7.
- Kastan, M. B., Q. Zhan, W. S. el-Deiry, F. Carrier, T. Jacks, W. V. Walsh, B. S. Plunkett, B. Vogelstein, and A. J. Fornace, Jr. 1992. A mammalian cell cycle checkpoint pathway utilizing $p53$ and GADD45 is defective in ataxia-telangiectasia. *Cell* **71**:587–597.
- Keegan, K. S., D. A. Holtzman, A. W. Plug, E. R. Christenson, E. E. Brainerd, G. Flagg, N. J. Bentley, E. M. Taylor, M. S. Meyn, S. B. Moss, A. M. Carr, T. Ashley, and M. F. Hoekstra. 1996. The *Atr* and *Atm* protein kinases associate with different sites along meiotically pairing chromosomes. *Genes Dev.* **10**:2423–2437.
- Khanna, K. K., and M. F. Lavin. 1993. Ionizing radiation and UV induction of $p53$ protein by different pathways in ataxia-telangiectasia cells. *Oncogene* **8**:3307–3312.
- Kuerbitz, S. J., B. S. Plunkett, W. V. Walsh, and M. B. Kastan. 1992. Wild-type $p53$ is a cell cycle checkpoint determinant following irradiation. *Proc. Natl. Acad. Sci. USA* **89**:7491–7495.
- Kuljis, R. O., Y. Xu, M. C. Aguila, and D. Baltimore. 1997. Degeneration of neurons, synapses, and neuropil and glial activation in a murine *Atm* knockout model of ataxia-telangiectasia. *Proc. Natl. Acad. Sci. USA* **94**:12688–12693.
- Lehmann, A. R. 1982. Pages 83–102. In B. A. Bridges and D. G. Harnden (ed.), *Ataxia-telangiectasia: a cellular and molecular link between cancer, neuropathology and immune deficiency*. Wiley Interscience, Chichester, United Kingdom.
- Macleod, K. F., N. Sherry, G. Hannon, D. Beach, T. Tokino, K. Kinzler, B. Vogelstein, and T. Jacks. 1995. $p53$ -dependent and independent expression of $p21$ during cell growth, differentiation, and DNA damage. *Genes Dev.* **9**:935–944.
- Meyn, M. S. 1995. Ataxia-telangiectasia and cellular responses to DNA damage. *Cancer Res.* **55**:5991–6001.
- Nakanishi, M., G. R. Adami, R. S. Robetorye, A. Noda, S. F. Venable, D. Dimitrov, O. M. Pereira-Smith, and J. R. Smith. 1995. Exit from G0 and entry into the cell cycle of cells expressing $p21^{Sdi1}$ antisense RNA. *Proc. Natl. Acad. Sci. USA* **92**:4352–4356.
- Noda, A., Y. Ning, S. F. Venable, O. M. Pereira-Smith, and J. R. Smith. 1994. Cloning of senescent cell-derived inhibitors of DNA synthesis using an expression screen. *Exp. Cell Res.* **211**:90–98.
- Parker, S. B., G. Eichele, P. Zhang, A. Rawls, A. T. Sands, A. Bradley, E. N. Olson, J. W. Harper, and S. J. Elledge. 1995. $p53$ -independent expression of $p21^{Cip1}$ in muscle and other terminally differentiating cells. *Science* **267**:1024–1027. (Comments.)
- Savitsky, T., et al. 1995. A single ataxia telangiectasia gene with a product similar to PI-3 kinase. *Science* **268**:1749–1753.
- Shiloh, Y. 1995. Ataxia-telangiectasia: closer to unraveling the mystery. *Eur. J. Hum. Genet.* **3**:116–138.
- Wang, Y. A., A. Elson, and P. Leder. 1997. Loss of $p21$ increases sensitivity to ionizing radiation and delays the onset of lymphoma in *atm*-deficient mice. *Proc. Natl. Acad. Sci. USA* **94**:14590–14515.
- Westphal, C. H., S. Rowan, C. Schmaltz, A. Elson, D. E. Fisher, and P. Leder. 1997. *atm* and $p53$ cooperate in apoptosis and suppression of tumorigenesis, but not in resistance to acute radiation toxicity. *Nat. Genet.* **16**:397–401.
- Xiong, Y., G. J. Hannon, H. Zhang, D. Casso, R. Kobayashi, and D. Beach. 1993. $p21$ is a universal inhibitor of cyclin kinases. *Nature* **366**:701–704.
- Xu, Y., T. Ashley, E. E. Brainerd, R. T. Bronson, M. S. Meyn, and D. Baltimore. 1996. Targeted disruption of *ATM* leads to growth retardation, chromosomal fragmentation during meiosis, immune defects, and thymic lymphoma. *Genes Dev.* **10**:2411–2422.
- Xu, Y., M. Baldassare, P. Fisher, G. Rathbun, E. M. Oltz, G. D. Yancopoulos, T. M. Jessell, and F. W. Alt. 1993. *LH-2*: a LIM/homeodomain gene expressed in developing lymphocytes and neural cells. *Proc. Natl. Acad. Sci. USA* **90**:227–231.
- Xu, Y., and D. Baltimore. 1996. Dual roles of *ATM* in the cellular response to radiation and in cell growth control. *Genes Dev.* **10**:2401–2410.
- Xu, Y. Unpublished data.
- Zakian, V. A. 1995. *ATM*-related genes: what do they tell us about functions of the human gene? *Cell* **82**:685–687.